Characterizing Single-Channel Behavior of GluA3 Receptors

Kinning Poon, Linda M. Nowak,[△] and Robert E. Oswald[△*]
Department of Molecular Medicine, Cornell University, Ithaca, New York

ABSTRACT AMPA receptors play a major role in excitatory neurotransmission in the CNS and are involved in numerous neurological disorders. Agonists bind to each of four bilobed LBDs of this tetrameric receptor, and upon binding, the lobes close to envelope the agonist, leading to channel activation. However, AMPA receptors exhibit complex activation kinetics, the mechanism of which has not yet been determined. We report here single-channel studies of a homomeric AMPA receptor (GluA3) activated by the full agonist, glutamate, and a partial agonist, fluorowillardiine. Both agonists activate the channel to the same three open conductance levels but with different open probabilities in each level. The closed probability (P_c) varied within records, particularly at low agonist concentrations. By sorting discrete segments of the record according to P_c using the X-means algorithm, we defined five modes of activity. The kinetic behavior could then be analyzed for both agonists over a range of agonist concentrations with a relatively simple model (three closed states and two open states for each open conductance level). The structural mechanism underlying the modal behavior is not clear; however, it occurs on a timescale consistent with hydrogen bonding across the lobe interface in the LBD.

INTRODUCTION

AMPA receptors, a subtype of ligand-gated ionotropic glutamate receptors (iGluAs), not only mediate the majority of excitatory neurotransmission in the CNS (1–4), they also play a role in peripheral function (5,6). Dysfunction of these receptors is associated with neurological diseases such as amyotropic lateral sclerosis and Huntington's disease, and disorders such as epilepsy and ischemic brain damage (7–9). The development of effective therapeutics is hampered by the widespread CNS distribution of AMPA receptors and the lack of a clear understanding of the role of specific subtypes in neuropathologies. Understanding the functional characteristics of AMPA receptors could reveal differences between subunits and allow for the design of selective pharmacological agents that target aberrant behavior without abolishing normal function.

The four AMPA subunits (GluA1–4) can form functional homo- or heterotetrameric channels (1,10). Each subunit has an LBD that is capable of binding one agonist molecule, a transmembrane domain that is responsible for channel gating, an extracellular N-terminal domain, and an intracellular C-terminal domain (1,2,11). Glutamate binding to the LBD leads to opening of the ion channel and a positive inward current, consisting of Na^+, K^+, and, depending on subunit composition and RNA editing (12), Ca^{2+} (13–15). The rate of desensitization is determined in part by a short sequence in the LBD called the flip/flop region (16); the flop form desensitizes faster than the flip form (17,18). In the case of the flip form, desensitization can be slowed with the addition of CTZ, an allosteric modulator that stabilizes dimerization between two LBDs.

The structure of both the LBD (19) and the full-length tetrameric GluA2 receptor (20) has been determined, and closure of the LBD upon agonist binding is thought to trigger activation of the ion channel (19,21–24). Functional studies of AMPA receptors on the macroscopic level have suggested a complex gating scheme (25,26). However, macroscopic currents reveal average ion channel activation and deactivation from a large number of channels, sometimes masking details that can only be delineated with single-channel recording. Previous single-channel studies of various AMPA channels (23,26–29) were limited by heavy filtering of the data, channel rundown in the outside-out configuration, or recording of receptors from neuronal cells for which the subunit composition was not known. Earlier single-channel studies on other ion channel subtypes, such as NMDA (30) and GABA (31) channels, yielded considerable insight into channel kinetics and modal behaviors that have yet to be characterized in detail for AMPA receptors.

For the single-channel studies described here, we used homomeric GluA3 receptors in the cell-attached mode, which simplified our system while maintaining a physiological cytoplasmic milieu. We used the physiological agonist glutamate and a partial agonist, fluorowillariine (FW). The use of partial agonists has been extremely important in the comparison of functional data with the extensive structural and dynamic information available for AMPA receptors (20,23,32,33). We report the number of conductance levels,

Submitted May 12, 2010, and accepted for publication June 29, 2010.

[△]Linda M. Nowak and Robert E. Oswald contributed equally to this work.

*Correspondence: reo1@cornell.edu

Abbreviations used: AMPA, α-amino-3-hydroxy-5-methyl-4-isoxazole-propionic acid; CNS, central nervous system; CTZ, cyclothiazide; FW, (*S*)-5-fluorowillardiine; flip and flop, alternatively spliced versions of AMPA receptors that vary in rates of desensitization and sensitivity to allosteric modulators; GluA1-4, four subtypes of AMPA receptor; GluN, NMDA receptor; LBD, extracellular ligand-binding domain of GluA2 and GluA3; LL, log likelihood; MIL, maximum interval likelihood; NMDA, N-methyl-D-aspartic acid; SKM, segmental-k-means.

Editor: Hassane Mchaourab.

0006-3495/10/09/1437/10 $2.00

doi: 10.1016/j.bpj.2010.06.058

the minimum number of states in each conductance class, the open probability, the mean lifetimes of channel opening, modal behaviors based on open probability, and a model describing the activation mechanism. Glutamate and FW share a common mechanism of channel activation with the same open conductance levels but with different open probabilities in each level. In the presence of either agonist, concentration-dependent modal behaviors that range from a mostly inactive to a highly active channel were observed.

MATERIALS AND METHODS

Cell culture

Human embryonic kidney 293 cells were stably transfected with GluA3i (G) (S.M. Holley and L.M. Nowak, unpublished). The receptor is the flip variant and has a G in the R/G editing site. The cells were cultured in Dulbecco's modified Eagle's medium containing 10% fetal bovine serum, 1% penicillin-streptomycin, and 1 μg/mL blasticidin, pH 7.4. The addition of the antibiotic, blasticidin, in the culture media selects for the growth of cells that express GluA3 channels. Cells were passaged every 3–4 days and used within 48 h after passage. All cultures were maintained in a 37°C incubator with 5% CO_2.

Acquisition of single-channel currents

All experiments were performed at room temperature (~23°C). Pipettes were pulled from thick-walled borosilicate glass with filament (Sutter Instrument Company, Novato, CA) to a resistance of 15–20 MΩ and fire-polished. Solutions were buffered at pH 7.4 and filtered using a 2 μM sterile filtering system (Corning, Lowell, MA). The bath buffer was a 1× Dulbecco's phosphate saline buffer with either Ca^{2+} and Mg^{2+}, or Mg^{2+} only (Invitrogen, Carlsbad, CA). The pipette solution contained (in mM) 150 NaCl, 10 Hepes/NaOH, 2 KCl. Stock solutions of glutamate or FW (Tocris Bioscience, Ellisville, MO) were made from the pipette solution and kept frozen in aliquots at −20°C until the day of the experiment. CTZ (Tocris Bioscience, Ellisville, MO, or Ascent Scientific, Princeton, NJ) was dissolved in methanol, frozen as 50 mM stock solutions, and added (100–150 μM) to all agonist-containing pipette solutions.

Single-channel currents were amplified at a gain of 100 mV/pA with an EPC-7 amplifier, low-pass filtered to 10 kHz using an external eight-pole Bessel filter, and digitized at 20 kHz using pClamp 7 software (Molecular Devices, Sunnyvale, CA). Data were converted from abf to qdf format on QuB software (http://www.qub.buffalo.edu) for analysis.

Single-channel currents were recorded for 2–10 min in the cell-attached mode with pipette holding potentials of +80 to +120 mV. To determine single-channel conductance, the current amplitude was measured in 20 mV increments, between −100 mV and +120 mV. The single-channel conductance was estimated as the slope of the current-voltage relationship. Open channel noise with a root mean-square deviation of ~0.2 pA and a frequency of 1.3–2 kHz was occasionally observed using both FW and glutamate as agonists. This was likely due to a variable amount of rapid channel blocking, but was small enough to have little effect on the analysis.

Analysis of single-channel data

Number of conductance levels

We defined the baseline by choosing a segment of the record without channel activity using QuB. We initially tested the criteria to use for analysis, which included the number of open conductance levels, by idealizing the data assuming up to four different conductance levels, filtering at frequencies ranging from 1 to 10 kHz, and altering the dead time at a range of 50–200 μs. We then analyzed the results from different combinations of criteria, and the criteria that provided the best fits to the amplitude histogram, dwell time histograms, and the largest LL units were used for all subsequent analyses. In all cases, three open conductance levels provided the best fits to the data (see Fig. S1 in the Supporting Material). The addition of a fourth open conductance level consistently exhibited a lower LL despite the increase in free parameters (see Fig. S1). Only records with one channel were chosen for further analysis.

Idealization and modeling of data

The amplitude for each open conductance level was estimated using the Amps function from QuB (Baum-Welch algorithm (34)). Next, the file was idealized at a dead time of 150 μs using the SKM algorithm (35) to an initial simple linear model, C↔O1↔O2↔O3 (Fig. 1 *A*), consisting of one closed and three open classes starting with all rates set to 100 s^{-1}. The data were analyzed with or without an additional 5 kHz filtering (effective filter of 4.5 kHz). With filtering greater than this (e.g., 2 kHz), baseline noise was often mistaken for small openings by QuB (Fig. S1). A dead time of 200 μs was imposed with the patches that had additional filtering. A MIL analysis (36) was applied on this initial model to determine the fit to the dwell time histograms. States were then added one at a time to each closed and open class, reidealized, refitted using MIL, and retained if the fits to the histograms improved and/or if the LL units increased by >10 LL units. If the addition of a state increased the LL by 10 but the rates to the new state were either close to zero or unrealistically large, the additional state was omitted. Because of the complex behavior of GluA3 channels, this method was applied to determine the least-complex kinetic model. This process was repeated again with rates starting at 10 s^{-1} to confirm that the final model and final rates were not affected by the starting values. Based on earlier studies of glutamate receptors, it is thought that at least two bound agonists are required to open the channel (11). In this case, three closed states might reflect a channel that has 0, 1, and 2 subunits with open channel gates. The fourth and sometimes a fifth closed state would reflect a deactivated or desensitized state. Our final model (Fig. 1 *B*) consists of three closed states and two open states in each of the open conductance levels. Loops that additionally connected closed states to the intermediate or large conductance levels in the model were tested, but in most cases worsened the fit to the dwell time histograms and/or gave unrealistic rates, so loops were not considered in our final model. Based on the transition matrices, transitions between the closed and the intermediate or large conductance levels were infrequently observed. Therefore, the final model does not include these transitions.

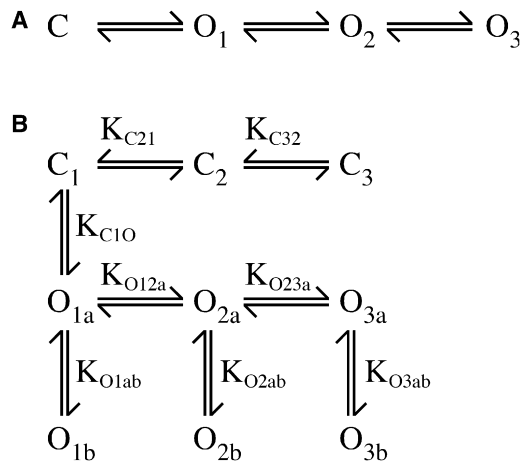

FIGURE 1 (*A*) Initial kinetic model that was used as a starting point but was found not to describe the data adequately. (*B*) Final kinetic model. The notation for the equilibrium is as follows: $K_{C21} = k_{C2\to C1}/k_{C1\to C2}$, $K_{O12a} = k_{O1a\to O2a}/k_{O2a\to O1a}$, $K_{O1ab} = k_{O1a\to O1b}/k_{O1b\to O1a}$, etc.

Segmentation of data

Inspection of the idealized traces indicated that most patches exhibited changes in activity over time, suggesting that the modal behavior observed for NMDA receptors (30) may also be a characteristic of AMPA receptors. Several different approaches were tested for sorting segments with different gating modes, including segmenting the data to 1 s segments or sorting based on mean open time (30). However, these approaches did not result in an improvement of LL within the segments. The patches that did contain activity changes had long closures between bursts. These long closures account for the fourth and sometimes fifth closed states, in similarity to previous findings (28). A critical time (t_{crit}), which describes the minimum closed duration between two bursts, was defined as described by Magleby and Pallotta (37), i.e., t_{crit} was defined by solving the following equation:

$$a_1 e^{-t_{crit}/\tau_1} = a_2\left(1 - e^{-t_{crit}/\tau_2}\right).$$

where a_2 and τ_2 describe the shortest closed component between bursts, and a_1 and τ_1 describe the longest closed component within a burst. This choice of t_{crit} equalizes the number of closed intervals in the two components that are misclassified. It was applied only to records with more than three closed components, and a_2 and τ_2 refer to the longest of the three shortest closed time components in the distribution. Closed times equal to or longer than t_{crit} were discarded in long records to yield isolated segments of bursts. These newly separated clusters were reidealized to one closed and three open conductance classes (Fig. 1 *A*) to determine the closed and open probabilities of each segment. The segments were then sorted into modes using the select function in QuB. The select function uses an X-means algorithm (38) to place each segment into the appropriate mode based on P_c (P_c was used instead of P_o because of the multiple conductance levels of the channel). The value of X is used to determine the number of modes by sorting the segments into similar clusters until the assignments stabilize. The modes were analyzed individually using the model described above (Fig. 1 *B*). Thus, the model in Fig. 1 *B* was applied to individual segments of data after removal of t_{crit} and sorted into modes using the X-means algorithm. In a few records having only three closed states and one mode, the model in Fig. 1 *B* was applied to the entire record. The files that exhibited modal behavior did not always contain all five modes, and often contained a combination of less than five modes. The dwell times of similar modes were averaged, but each mode was modeled separately. Table S1 summarizes each record analyzed, indicating which were segmented into modes and which were analyzed as a whole. Because the number of events in each group was necessarily less than the total number of events in the record, the LL was normalized to the number of events (LL/event) and each group was compared with the whole record. The final LL/event for each group ranged from 4.7 to 5.20, which is higher than that for the record as a whole by 0.05–0.30 LL/event. Five distinct modes were observed.

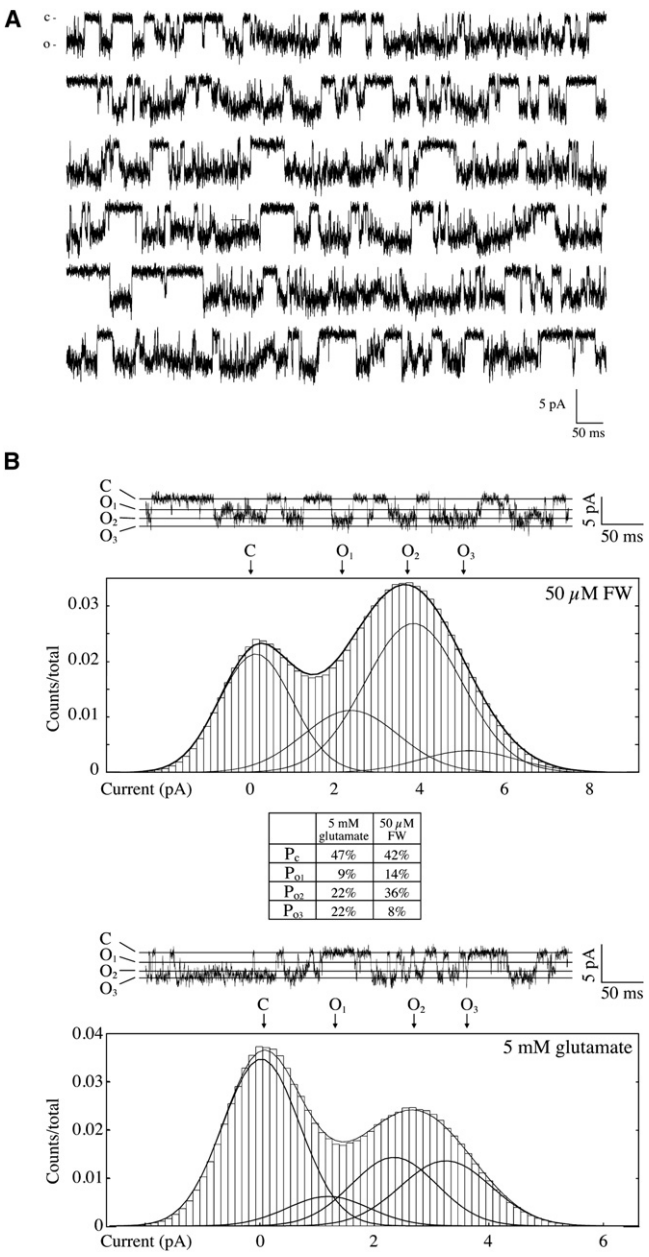

FIGURE 2 (*A*) A representative 6-s segment of a single-channel record of GluA3 activated by 50 μM FW. In this and all subsequent figures, the channel opens in a downward direction. (*B*) Amplitude histograms for an entire record obtained with 50 μM FW at 100 mV (*top*) and another obtained with 5 mM glutamate at 80 mV (*bottom*). Above each histogram is a representative 500-ms segment of the single-channel record with each of the three conductance levels indicated. The inset gives the percentage of each conductance level determined from a fit of four Gaussians to the amplitude histograms. For both the FW and glutamate records shown, the channel only exhibited M mode.

RESULTS

GluA3 channels open to three distinct conductance levels

A continuous 6-s segment of GluA3 single-channel data recorded with 50 μM FW is shown in Fig. 2 *A*. As described in Materials and Methods, the largest LL value was obtained with a model that contained three open conductance levels (Fig. S1 and Fig. S2), which is in agreement with most previous studies on GluA2 (23,28), GluA4 (28), GluA3 chimeras (11), and AMPA channels in granule cells (26,27), although four levels have been reported (40). The different conductance levels were distinguished from multichannel patches because patches containing two or more active channels had at least double the number of open levels, were rarely closed, and exhibited an amplitude that was twice the largest conductance of the single-channel patch. Also, double openings are readily identified in the presence of CTZ because the channel has a high P_o (17).

Amplitude probability density functions for 50 μM FW and 5 mM glutamate (both concentrations are above the corresponding EC_{50} (17,23,41)) bound to a single GluA3 channel are shown in Fig. 2 *B*. In addition to a closed level, three open current amplitude with conductance estimates of 14 $\pm$ 0.6 ($n = 6$), 26 $\pm$ 1.4 ($n = 3$), and 35 $\pm$ 1.8 ($n = 2$) pS for FW and 14 $\pm$ 2.2 ($n = 3$), 26 $\pm$ 1.3 ($n = 3$), and 39 $\pm$ 0.8 ($n = 3$) pS for glutamate (O_1, small; O_2, intermediate; and O_3, large, respectively; n is the number of records used for the measurement; Fig. S2) were observed for both FW and glutamate. However, the channel preferentially opens to the intermediate and large conductance levels when bound to glutamate, and to the small and intermediate conductance levels when bound to FW (Fig. 2 *B*, *inset*). The presence of the same three conductance levels in both full and partial agonists is consistent with similar activation schemes.

GluA3 single-channel currents fit to a simple model

The simplest model with the highest LL value determined from MIL analysis consists of two open states in each conductance class and three closed states (Fig. 1 *B*). Dwell time histograms recorded with saturating concentrations of FW (50 μM) and glutamate (5 mM) are shown in Fig. 3. The open histograms demonstrate the presence of two exponentials (consistent with the two open states used in the MIL modeling), in similarity to previous studies (28). Adding loops between states resulted in either distortion of the fit to the dwell time histogram or rate constants that were either unrealistically high or close to zero. A state transition matrix from the two patches that describes the percentage of transitions between states is given in Table 1. Based on transition matrices from all analyzed patches, the channel favors transitions between adjacent levels (stepwise opening and closing). These results are also in agreement with Zhang et al. (29), who reported transitions between adjacent levels for GluA2 wild-type and T686 mutant.

At least three closed states are necessary to fit the data (Table S2). In some cases, depending upon the concentration of agonist, a fourth and fifth closed state can be detected. Previous studies on homomeric GluA2 and GluA4 channels detected four closed dwell times (29,42). Patches acquired at high concentrations of agonist were uniform in activity. These patches usually had three and sometimes a fourth closed state. At high concentrations when four closed states were observed, the long closures likely reflect a desensitized state, for the following reasons: 1) at high concentrations of agonist, the receptor is saturated with agonist for so long that closures do not represent unbound receptor; 2), due to the cell-attached patch configuration, the agonist is at equilibrium with the binding sites; 3), the recordings are relatively long, so it is expected that the

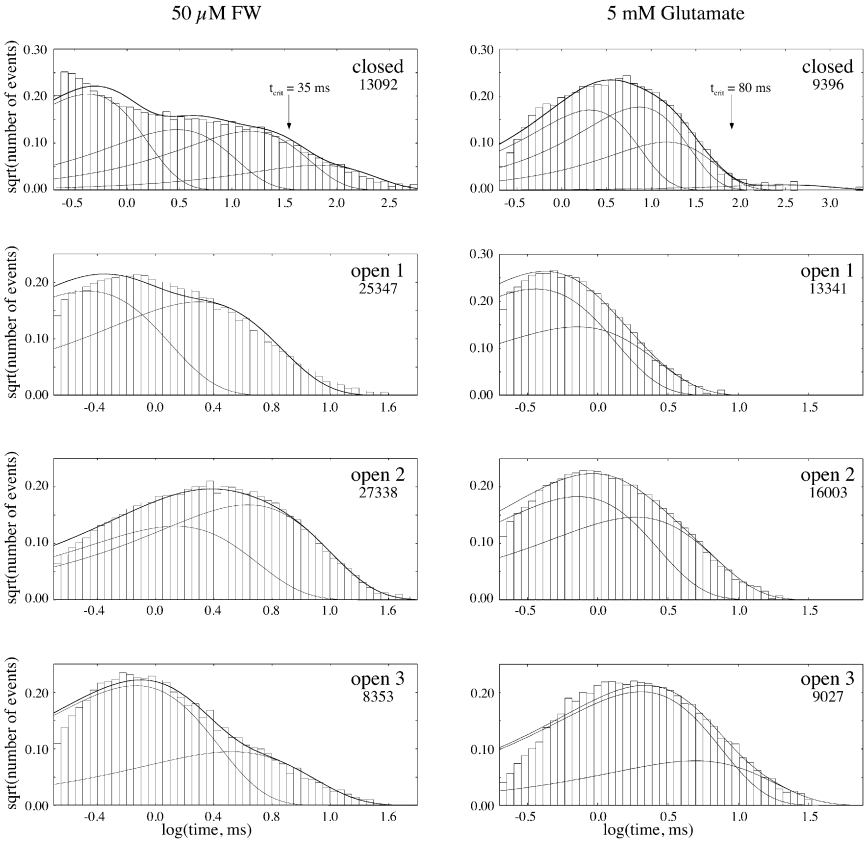

FIGURE 3 Dwell time histograms for the same records used to generate Fig. 2 *B*. The number in the upper-left corner indicates the number of events.

TABLE 1 State transition matrices

	50 μM FW					5 mM glutamate			
	C	O_1	O_2	O_3		C	O_1	O_2	O_3
C	-	13.2	6.8	0.4	C	-	13.6	4.7	0.7
O_1	13.4	-	18.5	1.6	O_1	13.9	-	13.8	1.7
O_2	6.6	18.8	-	9.4	O_2	4.4	13.7	-	15.5
O_3	0.5	1.4	9.5	-	O_3	0.8	2.1	15.0	-

State transition matrices showing the percentage of transitions between each conductance level. Transitions between adjacent states are far more frequent than transitions between nonadjacent states. This constrains the model shown in Fig. 1 such that transitions between closed states and O_2, between closed states and O_3, and between O_1 and O_3 are not included.

channel would eventually desensitize, as CTZ slows but does not abolish desensitization. At lower concentrations of agonist, four or five closed states were observed. Since lower concentrations may reflect a nonsaturated receptor, one of the closed times could represent deactivation. To investigate whether removal of these long closures caused an alteration in the measured parameters, we compared the dwell time constants of patches with and without the long closures. The shortest three dwell time constants for the closed state and the dwell time constants for the open states were similar before and after the long closures were discarded. For records with four or five closed states, the critical time (t_{crit}; see Materials and Methods) was determined, and closures longer than t_{crit} were discarded.

Analysis of modal behavior

Evidence for modal behavior as a function of concentration

The number of open states, as well as the final model, was consistent across all patches. Most patches acquired at lower concentrations of agonist exhibited fluctuation in activity over time. Analysis of patches at lower agonist concentrations as a whole did not yield fits that overlaid well to the dwell time histograms. Inspection of the records suggested that, over time, the channel operated in modes that changed abruptly from one to another, with the possibility that the rate constants differed in the various modes (Figs. 4 and 5). Although a number of methods were tested for sorting records into different modes, the most successful approach was based on P_c. Bursts were separated into segments based on the t_{crit} value (see Materials and Methods), with lower concentrations of agonist having the largest range of t_{crit} values between different files (1 mM Glu 79–182 ms, 200 μM Glu 78–309 ms, 100 μM Glu 50–365 ms, 200 μM FW 73 ms, 50 μM FW 36–87 ms, 10 μM FW 53–145 ms, and 5 μM FW 53–348 ms). Bursts with similar activity (based on P_c) were clustered together and analyzed separately (e.g., Fig. 4 *B*). The closed channel probability (P_c), the open channel probability (P_o) in each separate conductance class, and the length of time spent in each conductance class varied among modes.

Five modes were observed for the full and partial agonist (very high (VH), high (H), medium (M), low (L), and very low (VL) modes) corresponding to P_o (i.e., $1 - P_c$) of approximately >90%, 70%, 50%, 30%, and <20%. Although up to five different modes were detected using the X-means algorithm, the frequency of observing these modes varied with the agonist and the agonist concentration, and not all records contained all five modes (Table S1). Fig. 4 shows three different patches acquired at 500, 50, and 10 μM FW, and the modes exhibited in each patch. For each mode, the kinetic properties were similar regardless of the agonist concentration. In Fig. 5 *A*, the P_o values ($1 - P_c$) for sequential segments of one record are shown (10 μM FW). The classification into modes is indicated by the plotting symbol in Fig. 5 *A*, and the mode for each segment is given in the corresponding plot in Fig. 5 *B*. The inset shows a modal transition matrix, demonstrating that the channel is more likely to remain in the same mode than to transition to a different mode.

At very high concentrations of FW, the channel had a $P_o >$ 90% and mostly resided in the VH mode of activity throughout the record. At 500 μM FW, the average P_o was 95% ($n = 5$) for all of the patches. At 200 μM FW, two out of three patches had a VH mode of activation and the third patch had a mixture of VH, H, and M. As the agonist concentration was decreased, lower probability modes were more frequently observed. At 50 μM FW, the majority of the patches had a mixture of VH ($n = 4$), H ($n = 2$), and M ($n = 1$) modes. We also began to observe an L mode of activity at 50 μM FW, but with too few events to analyze.

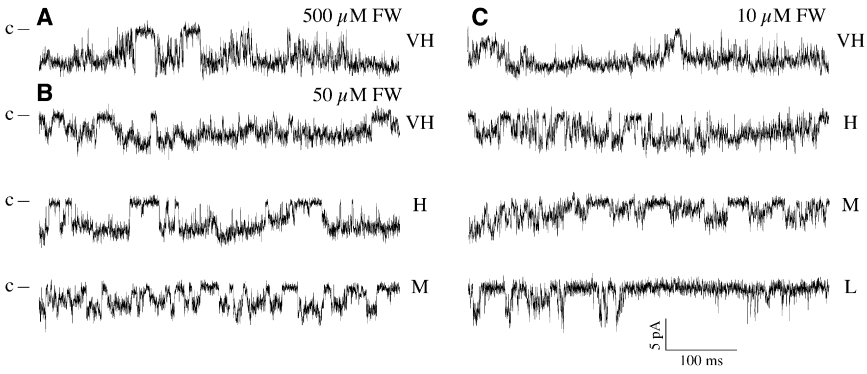

FIGURE 4 Representative segments of single-channel records obtained with (*A*) 500 μM, (*B*) 50 μM, and (*C*) 10 μM FW showing different modes of activity (VH, H, M, and L).

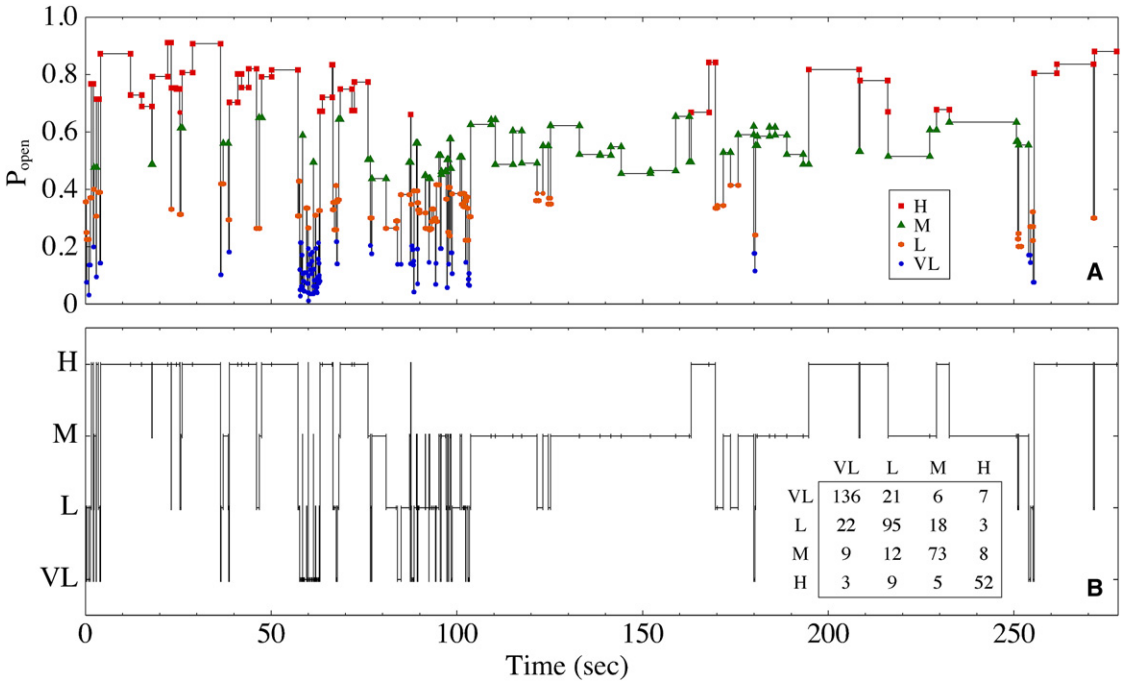

FIGURE 5 (*A*) P_o for segments of a single-channel record with 50 μM FW. Closed times greater than t_{crit} were removed, and the horizontal lines indicate the length of the segment at a given P_o (*y* axis). The plotting symbol at the beginning and end of a segment indicates the mode as defined in the legend. (*B*) The same segment as in panel *A* but classified according to mode instead of P_o. The inset is a modal transition matrix for the modes.

Most of the patches recorded with 10 μM FW displayed more than one mode of activation, which consisted of an assortment of all five modes: VH ($n = 1$), H ($n = 5$), M ($n = 3$), L ($n = 2$), and VL ($n = 3$). The application of 5 μM FW for two out of seven patches resulted in the activation of the channel to all but the VH mode. The other five patches displayed activation mainly to the lowest conductance level (see "Nonbinomial activation to a single conductance level" below).

Modal behaviors follow a binomial distribution

Previous analyses of single-channel events from GluA2 suggested that the channel opens to multiple levels and the openings follow a binominal distribution (23); that is, once bound with a given number of agonist molecules (two to four), the channel can display openings to up to three levels. The four levels (closed plus three open) can be viewed as four trials (n), and the level of a particular opening is defined as the number of successes (k). The probability of success (p) can then vary between agonists, at different concentrations, and, in this case, in different modes. As shown in Table 2, p (also referred to as the efficacy factor (23)) is consistent across modes and increases from VL to VH mode.

Variation among modes

In VH mode, the open dwell times (τ_o) in the open states of all conductance levels are longer and decrease as the modal activity decreases. Generally, the VH mode has the longest τ_o-values whereas the VL mode has the shortest dwell times for all the conductance levels (Table S2). This is true for channels activated by both FW and glutamate. With the exception of the longest closed dwell time (τ_c), which may have been affected by discarding the long closures, the shortest τ_c-values were relatively similar among all modes and concentrations. After MIL modeling was completed, equilibrium constants calculated from the rate constants ($K = k_f/k_r$) for the same modes were averaged across patches (Table S3). Overall, for the step that represents the transition from closed to open, the equilibrium constant (K_{C1O}; see Fig. 1 for the definition of the equilibrium constants) varies between modes, being greatest for the VH and lowest for the VL mode at all concentrations for both glutamate and FW (Table S3). K_{O12a} and K_{O23a} are slightly larger for bound glutamate than for FW, indicating that the energy barrier

TABLE 2 Efficacy factors for modes

	FW	Glutamate
VH	0.66 ± 0.02	0.73 ± 0.04
H	0.60 ± 0.02	0.71 ± 0.05
M	0.45 ± 0.05	0.59 ± 0.08
L	0.26 ± 0.11	0.42 ± 0.05
VL	0.24 ± 0.08	0.42 ± 0.11

The efficacy factor (p) was calculated as described in Materials and Methods based on the conductance histograms for records separated into specific modes. The concentrations used ranged from 5 to 500 μM for FW, and from 50 to 5000 μM for glutamate. The efficacy factor is synonymous with the probability of success in a bionomial distribution. The higher the value, the more likely a gate will be open.

for opening in the presence of glutamate is lower. The distribution in each conductance level is independent of agonist concentration and is dependent on the mode. The distribution shifts toward the lower conductance states in the lower modes of activation. The O_3 level is the least populated in all modes for FW relative to glutamate.

Transitions between modes

The long closures between bursts represented periods of channel inactivity that may be due to desensitization and/or deactivation. To determine whether the channel entered modes randomly after a long closure or if we observed specific transitions, we generated a modal transition matrix for each record. These results showed that the channel preferentially remains in the same mode after a long closure, and when a transition to a different mode is observed, it is preferentially to an adjacent mode (Fig. 5 *B*, *inset*).

Nonbinomial activation to a single conductance level

In several cases, the channel opened to an individual conductance level with few or no transitions to other levels. In the presence of 200 μM glutamate, six patches exhibited the largest conductance level without any transitions to the smallest and intermediate levels (Fig. S3 *A*). Four of these patches had a VH mode of activity ($P_o = 93.5\% \pm 0.03$) and long mean lifetime of channel opening (25–145 ms). Because of this high activity and long duration openings, events (transitions between open and closed) were few in number and the MIL analysis was limited. The remaining two patches had a mixture of H, M, and VL modes, or only L mode, despite exhibiting only the highest conductance level.

In the case of FW, patches that exhibited mainly one conductance were largely in the lowest conductance level. This included five of seven records with 5 μM FW (Fig. S3 *B*), as well as single records at 50, 200, and 500 μM. At 5 μM FW, three out of five patches exhibited VH mode while remaining in the lowest conductance state for 80% of the record. The remainder of these records showed other modes but remained largely in the lowest conductance state. These records and those of glutamate cited above do not follow a binomial distribution and clearly represent an aspect of channel gating that differs from that observed in the majority of the recordings from GluA3 channels.

DISCUSSION

Although a great deal is known concerning the structure of AMPA receptors (20,43), the details of channel activation are complex and less well characterized. This complexity arises at least in part from time-dependent changes in activity that vary with agonist concentration. Although an excess of high-conductance openings at low glutamate concentrations in short records has been associated with two modes of activity (40), time-dependent changes in activity appear to be more complex and consist of a number of different modes that vary with agonist concentration.

Homomeric GluA3 channels have three open conductance classes, which are shared by the full agonist, glutamate, and the partial agonist, FW. This is in agreement with previous studies (11,23,29). We show here that at high concentrations, the channel can be modeled as three closed states and three conductance levels, each with two kinetically distinct open states. At lower concentrations, the channels can be modeled with a similar number of states, but the fit to the data is not as good as at high concentrations, and the probability of opening seems to vary within a given record. As has been described for GluN and GABA channels (30,31), dividing the record into segments (in this case, grouping segments based on P_c using the X-means function in QuB) produced much higher LL/event values for dwell time fits. Using a range of FW and glutamate concentrations, we defined five modes of activity (see Fig. 5). The distribution of openings was consistent within each mode regardless of concentration, and the probability of observing modes of higher activity increased with increasing agonist concentration. Modeling the openings as a binomial, the efficacy factor (23), p, is larger in higher modes. Furthermore, analysis of the modal behavior suggested that the channel preferentially remains in the same mode after a long closure or changes to an adjacent mode.

The question then is, what is the nature of the modal behavior? Our results clearly show that it is a graded process, with higher modes associated with higher agonist concentration and higher conductances. One possibility is that modal gating is tied to occupancy level; that is, the number of agonists bound and perhaps the distribution of bound LBDs within the tetramer may determine the mode, such that the lowest modes would have the lowest occupancy. Since the highest conductance is observed, albeit with low probability, even in VL mode, this model would suggest that the highest conductance level could be produced by tetramers that are only partially occupied by agonist. The structural basis of such a model is not obvious. Alternatively, the conductance levels could be set by the number of occupied subunits for which the LBD is in the closed lobe conformation. However, in its simplest form, this model does not explain modal gating. To account for modal gating, at least one additional factor would have to be controlling gating behavior. Although factors such as phosphorylation could play a role, at least two processes associated with the LBD could contribute to modal behavior. These include hydrogen bonding across the lobe interface and the binding of CTZ.

Extensive studies of the GluA2 LBD (21,23,32,33), supported by recent crystal structures of the GluA3 LBD (44), show that two H-bonds can form across the dimer interface, stabilizing the closed lobe form. However, the lobes can be

closed in the absence of these H-bonds, in which a 180° flip of the peptide bond between D655 and S656 (GluA3 numbering) occurs (21). Generally, the conformation in which the H-bonds can form is referred to as the flipped form, and the 180° rotation of the peptide bond that cannot form H-bonds is the unflipped form. Intermediate forms have also been observed (21). The flipped form of the peptide bond is a dynamic process that can occur in the presence of both FW and glutamate (32). Thus, the modes may be set by both the occupancy and the H-bonding state. The VH mode could be generated by the occupancy of all four subunits with three to four H-bonded subunits, whereas the lower modes would have progressively fewer H-bonds and a tendency toward lower occupation. Depending on the timescale of the H-bonding, a receptor could be locked into a particular mode for at least a burst of channel openings. An important issue is the timescale of the transition between the flipped and unflipped form of the peptide bond. This cannot be approached by crystallography. However, relaxation measurements by NMR suggest that at least for FW and glutamate, the process is longer than a few milliseconds (33). H/D exchange studies can provide an estimate of the timescale of the opening rate for the H-bond, but only at high pH (EX1 limit (45)). The rates measured at high pH are on the order of 10 Hz, which approaches the timescale necessary to account for the duration of the modes. Although rigorous fitting to a model with transient H-bonds that lock the LBD would not be possible with our single-channel data sets due to the relatively small number of transitions between modes, different modes can easily be simulated by an additional state with a locked lobe (i.e., no off-rate).

An additional factor that may contribute to modal behavior is the binding of CTZ. An intact dimer interface of the LBD is thought to be necessary for channel activation, and the dissociation of the interface is associated with desensitization (13). The status of the dimer interface in the resting state has been ambiguous. A recent study by Gonzalez et al. (46) suggested that the dimer interface is not intact in the resting state, and only forms with activation. This may mean that CTZ would bind preferentially to dimers, perhaps those with agonist in both LBDs. If this were true, it would be possible at low concentrations of agonist to obtain a mode with high levels of activation to a low conductance state by occupation of both monomers within a dimer, with CTZ bound to the dimer interface. Conversely, occupying one monomer of each potential dimer would not necessarily bind CTZ and could lead to a mode with low levels of activation.

An additional question relates to the nature of partial agonism and the transduction of the binding signal into gate opening. Clearly, the closure of an LBD is associated with channel activation; however, it is not clear exactly how the LBD is coupled to channel gating. That is, an individual LBD bound to agonist is assumed to be able to activate a channel gate that is associated with an increase in channel conductance. Activation only occurs if the LBD has an intact dimer interface with the adjacent LBD. Even in the case of an intact dimer interface, individual subunit gating is unlikely to be directly coupled to occupancy of the binding site. This was recognized by Jin et al. (23), and, as noted above, the efficacy factor was introduced to quantitate the lower efficacy of partial agonists. Jin et al. (23) suggested that the efficacy factor is determined by the degree to which the lobes of the LDB are closed, in that partial agonists exhibit lower degrees of lobe closure than full agonists in many crystal structures. This was consistent with the data at the time, but the structural link to channel gating remained unclear. Zhang et al. (29) proposed that channel activation is associated with the stability of the closed lobes, and Maltsev et al. (32) suggested that partial agonists have a distribution of lobe closures ranging from perhaps fully closed to more open. Based on recent NMR and crystallographic evidence that a full lobe closing of GluA2 LBD can be observed under some conditions with partial agonists (e.g., iodowillardiine and kainate; A. H. Ahmed and R. E. Oswald, unpublished observations), we suggest that the efficacy relates to the probability of a full lobe closure, and that in a given mode or distribution of LBD occupancy, the conductance level is set by the number of LBDs that are in the fully closed conformation at any given time. The LBDs that have formed H-bonds as described above would be transiently locked (on the timescale of 100 ms) in this fully closed-lobe conformation. FW is a relatively strong partial agonist, and one might expect that full lobe closure would be more likely than for a weaker partial agonist such as iodowillardiine or kainate. The occupancy in the conductance levels for FW is consistently lower than for the full agonist, glutamate, but the difference is not as dramatic as observed previously for iodowillardiine versus glutamate (23).

In addition to the modal behavior exhibited in the majority of records, occasionally openings to a single level (or largely a single level) were observed. In the case of glutamate, these openings were to the highest conductance levels, and with FW the openings were largely to the lowest conductance level. In at least one case, the activity changed from the typical three conductance levels to a single conductance within one record. These channels have the same conductance levels as GluA3 and have not been observed in the absence of agonist, and thus appear to be a distinct functional state of GluA3.

NMDA receptors, unlike AMPA receptors, require all four subunits to be bound to agonist (two of which are glycine-specific) for activation (47). Unlike the concentration dependence of modal behavior for GluA3, no such correlation exists for NMDA channels (30). Nevertheless, AMPA receptor activation shares some commonalities with NMDA receptor gating. Modeling of both channels requires three closed states, with one leading into an open

level, and two exponentials are needed to fit to the open level (30,48). Partial agonism at NMDA channels results in a decrease in the open channel probability of a single conductance level (49), whereas for AMPA channels, partial agonism is associated with a decrease in the open probability of the largest conductance levels. Thus, although NMDA receptors open to only a single conductance level, considerable similarities between the two classes of glutamate receptors are evident.

The single-channel results obtained with GluA3 suggest that the kinetic model of activation is simple, but the channel can exist in different modes depending, at least in part, on agonist occupation. All recordings were done in the presence of CTZ, which dramatically decreases the rate of desensitization. Nevertheless, one might expect the modal behavior to still have relevance to normal channel activation at the synapse. The half-time of desensitization of GluA3 is several milliseconds (13,50), so for a given excitatory postsynaptic potential the mode would not necessarily change for any given channel. However, the excitatory postsynaptic potential is made up of synchronous activation of thousands of channels, probably activating in a distribution of modes. The development of compounds that can favor high or low modes could be of therapeutic value for neurological disorders such as Alzheimer's disease (drugs favoring high modes) or epilepsy (drugs favoring low modes).

SUPPORTING MATERIAL

Three figures and three tables are available at http://www.biophysj.org/biophysj/supplemental/S0006-3495(10)00802-7.

The authors thank Dr. Sandra Holley (UCLA), Dr. Jayasri Srinivasan (Cornell), Dr. Gregory Weiland (Cornell), Dr. Gabriela Popescu (SUNY Buffalo), Dr. Fred Sachs (SUNY Buffalo), Dr. Anthony Auerbach (SUNY Buffalo), and Chris Nicolai (SUNY Buffalo) for helpful advice, technical support, and discussions.

This work was supported by a grant from the National Institutes of Health (R01 NS049223). K.P. was supported by a Ruth L. Kirschstein National Research Service Award (1F31NS063518).

REFERENCES

1. Dingledine, R., K. Borges, …, S. F. Traynelis. 1999. The glutamate receptor ion channels. *Pharmacol. Rev.* 51:7–61.
2. Hollmann, M., and S. Heinemann. 1994. Cloned glutamate receptors. *Annu. Rev. Neurosci.* 17:31–108.
3. Nakanishi, S., and M. Masu. 1994. Molecular diversity and functions of glutamate receptors. *Annu. Rev. Biophys. Biomol. Struct.* 23:319–348.
4. Sommer, B., and P. H. Seeburg. 1992. Glutamate receptor channels: novel properties and new clones. *Trends Pharmacol. Sci.* 13:291–296.
5. Weaver, C. D., T. L. Yao, …, T. A. Verdoorn. 1996. Differential expression of glutamate receptor subtypes in rat pancreatic islets. *J. Biol. Chem.* 271:12977–12984.
6. Gill, S. S., O. M. Pulido, …, P. F. McGuire. 1998. Molecular and immunochemical characterization of the ionotropic glutamate receptors in the rat heart. *Brain Res. Bull.* 46:429–434.
7. Kwak, S., and J. H. Weiss. 2006. Calcium-permeable AMPA channels in neurodegenerative disease and ischemia. *Curr. Opin. Neurobiol.* 16:281–287.
8. Chen, P. E., and D. J. Wyllie. 2006. Pharmacological insights obtained from structure-function studies of ionotropic glutamate receptors. *Br. J. Pharmacol.* 147:839–853.
9. Black, M. D. 2005. Therapeutic potential of positive AMPA modulators and their relationship to AMPA receptor subunits. A review of preclinical data. *Psychopharmacology (Berl.).* 179:154–163.
10. Madden, D. R. 2002. The structure and function of glutamate receptor ion channels. *Nat. Rev. Neurosci.* 3:91–101.
11. Rosenmund, C., Y. Stern-Bach, and C. F. Stevens. 1998. The tetrameric structure of a glutamate receptor channel. *Science.* 280:1596–1599.
12. Schmauss, C., and J. R. Howe. 2002. RNA editing of neurotransmitter receptors in the mammalian brain. *Sci. STKE.* 2002:pe26.
13. Sun, Y., R. Olson, …, E. Gouaux. 2002. Mechanism of glutamate receptor desensitization. *Nature.* 417:245–253.
14. Stern-Bach, Y., S. Russo, …, C. Rosenmund. 1998. A point mutation in the glutamate binding site blocks desensitization of AMPA receptors. *Neuron.* 21:907–918.
15. Paas, Y. 1998. The macro- and microarchitectures of the ligand-binding domain of glutamate receptors. *Trends Neurosci.* 21:117–125.
16. Sommer, B., K. Keinanen, …, P. H. Seeburg. 1990. Flip and flop: a cell-specific functional switch in glutamate-operated channels of the CNS. *Science.* 249:1580–1585.
17. Pei, W., Z. Huang, and L. Niu. 2007. GluR3 flip and flop: differences in channel opening kinetics. *Biochemistry.* 46:2027–2036.
18. Pei, W., Z. Huang, …, L. Niu. 2009. Flip and flop: a molecular determinant for AMPA receptor channel opening. *Biochemistry.* 48:3767–3777.
19. Armstrong, N., Y. Sun, …, E. Gouaux. 1998. Structure of a glutamate-receptor ligand-binding core in complex with kainate. *Nature.* 395:913–917.
20. Sobolevsky, A. I., M. P. Rosconi, and E. Gouaux. 2009. X-ray structure, symmetry and mechanism of an AMPA-subtype glutamate receptor. *Nature.* 462:745–756.
21. Armstrong, N., and E. Gouaux. 2000. Mechanisms for activation and antagonism of an AMPA-sensitive glutamate receptor: crystal structures of the GluR2 ligand binding core. *Neuron.* 28:165–181.
22. Gouaux, E. 2004. Structure and function of AMPA receptors. *J. Physiol.* 554:249–253.
23. Jin, R., T. G. Banke, …, E. Gouaux. 2003. Structural basis for partial agonist action at ionotropic glutamate receptors. *Nat. Neurosci.* 6:803–810.
24. Jin, R., and E. Gouaux. 2003. Probing the function, conformational plasticity, and dimer-dimer contacts of the GluR2 ligand-binding core: studies of 5-substituted willardiines and GluR2 S1S2 in the crystal. *Biochemistry.* 42:5201–5213.
25. Zhang, W., A. Robert, …, J. R. Howe. 2006. The relationship between agonist potency and AMPA receptor kinetics. *Biophys. J.* 91:1336–1346.
26. Smith, T. C., L. Y. Wang, and J. R. Howe. 2000. Heterogeneous conductance levels of native AMPA receptors. *J. Neurosci.* 20:2073–2085.
27. Smith, T. C., and J. R. Howe. 2000. Concentration-dependent substate behavior of native AMPA receptors. *Nat. Neurosci.* 3:992–997.
28. Swanson, G. T., R. W. Gereau, 4th, …, S. F. Heinemann. 1997. Identification of amino acid residues that control functional behavior in GluR5 and GluR6 kainate receptors. *Neuron.* 19:913–926.
29. Zhang, W., Y. Cho, …, J. R. Howe. 2008. Structural and single-channel results indicate that the rates of ligand binding domain closing and opening directly impact AMPA receptor gating. *J. Neurosci.* 28:932–943.
30. Popescu, G., and A. Auerbach. 2003. Modal gating of NMDA receptors and the shape of their synaptic response. *Nat. Neurosci.* 6:476–483.

31. Lema, G. M., and A. Auerbach. 2006. Modes and models of GABA(A) receptor gating. *J. Physiol.* 572:183–200.

32. Maltsev, A. S., A. H. Ahmed, …, R. E. Oswald. 2008. Mechanism of partial agonism at the GluR2 AMPA receptor: Measurements of lobe orientation in solution. *Biochemistry.* 47:10600–10610.

33. Fenwick, M. K., and R. E. Oswald. 2008. NMR spectroscopy of the ligand-binding core of ionotropic glutamate receptor 2 bound to 5-substituted willardiine partial agonists. *J. Mol. Biol.* 378:673–685.

34. Baum, L. E., T. Petrie, …, N. Weiss. 1970. A maximization technique occurring in the statistical analysis of probabilistic functions of Markov chains. *Ann. Math. Stat.* 41:164–171.

35. Qin, F., and L. Li. 2004. Model-based fitting of single-channel dwell-time distributions. *Biophys. J.* 87:1657–1671.

36. Qin, F., A. Auerbach, and F. Sachs. 1996. Estimating single-channel kinetic parameters from idealized patch-clamp data containing missed events. *Biophys. J.* 70:264–280.

37. Magleby, K. L., and B. S. Pallotta. 1983. Burst kinetics of single calcium-activated potassium channels in cultured rat muscle. *J. Physiol.* 344:605–623.

38. Pelleg, D., and A. W. Moore. 2000. X-means: extending K-means with efficient estimation of the number of clusters. Morgan Kaufmann Publishers, San Francisco, CA.

39. Reference deleted in proof.

40. Prieto, M. L., and L. P. Wollmuth. 2010. Gating modes in AMPA receptors. *J. Neurosci.* 30:4449–4459.

41. Patneau, D. K., M. L. Mayer, …, J. C. Watkins. 1992. Activation and desensitization of AMPA/kainate receptors by novel derivatives of willardiine. *J. Neurosci.* 12:595–606.

42. Swanson, G. T., S. K. Kamboj, and S. G. Cull-Candy. 1997. Single-channel properties of recombinant AMPA receptors depend on RNA editing, splice variation, and subunit composition. *J. Neurosci.* 17:58–69.

43. Kubo, M., and E. Ito. 2004. Structural dynamics of an ionotropic glutamate receptor. *Proteins.* 56:411–419.

44. Ahmed, A. H., Q. Wang, …, R. E. Oswald. 2009. Structure of the S1S2 glutamate binding domain of GLuR3. *Proteins.* 75:628–637.

45. Fenwick, M. K., and R. E. Oswald. 2010. On the mechanisms of α-amino-3-hydroxy-5-methylisoxazole-4-propionic acid (AMPA) receptor binding to glutamate and kainate. *J. Biol. Chem.* 285:12334–12343.

46. Gonzalez, J., M. Du, …, V. Jayaraman. 2010. Role of dimer interface in activation and desensitization in AMPA receptors. *Proc. Natl. Acad. Sci. USA.* 107:9891–9896.

47. Johnson, J. W., and P. Ascher. 1987. Glycine potentiates the NMDA response in cultured mouse brain neurons. *Nature.* 325:529–531.

48. Auerbach, A., and Y. Zhou. 2005. Gating reaction mechanisms for NMDA receptor channels. *J. Neurosci.* 25:7914–7923.

49. Kussius, C. L., A. M. Popescu, and G. K. Popescu. 2010. Agonist-specific gating of NMDA receptors. *Channels (Austin).* 4:78–82.

50. Robert, A., and J. R. Howe. 2003. How AMPA receptor desensitization depends on receptor occupancy. *J. Neurosci.* 23:847–858.